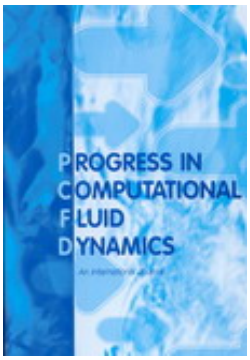

Progress in Computational Fluid Dynamics, An International Journal

ISSN online: 1741-5233 - ISSN print: 1468-4349
https://www.inderscience.com/pcfd

Investigation on the 1-kW Francis turbine elbow type draft tube performance by numerical and optimisation approach

Sathish Kalidas, Ramamoorthi Rangasamy, Venkatesh Seenivasan

DOI: 10.1504/PCFD.2021.10048084

Article History:

Received:	24 April 2021
Last revised:	10 November 2021
Accepted:	13 November 2021
Published online:	02 February 2023

Investigation on the 1-kW Francis turbine elbow type draft tube performance by numerical and optimisation approach

Sathish Kalidas*

Department of Mechanical Engineering,
Sri Eshwar College of Engineering,
Kinathukadavu, Coimbatore, Tamil Nadu, 641202, India
Email: sathishsece13@gmail.com
*Corresponding author

Ramamoorthi Rangasamy

Department of Mechanical Engineering,
Sri Krishna College of Engineering and Technology,
Kuniyamuthur, Coimbatore, Tamil Nadu, 641008, India
Email: ramamoorthi@skcet.ac.in

Venkatesh Seenivasan

Department of Mechanical Engineering,
National Institute of Technology,
Tiruchirappalli, Tamil Nadu, 620015, India
Email: venkatesme2014@gmail.com

Abstract: In this study, the performance of a 1-kW Francis turbine elbow-type draft tube is examined. Three geometric factors related to the draft tube, namely, the hose length, diffuser length, and exit diameter of the draft tube, are considered for improving the pressure recovery factor. The Taguchi method is applied to derive a regression equation related to these three parameters. The geometric factors of the draft tube are altered using a genetic algorithm (GA). The optimised draft tube is fabricated for the experimental investigation. The results indicate that using the optimised draft tube increases the overall efficiency. Moreover, it leads to an increase in the pressure recovery factor from 0.75 to 0.88. The pressure, velocity and kinetic energy flow fields were obtained using computational fluid dynamics (CFD) simulation. The shear stress transport k-ω model is applied for CFD simulation. The computed pressure recovery factor obtained from the CFD analysis is compared with that obtained from the experimental results. An acceptable range of accuracy is obtained in this study.

Keywords: elbow draft tube; pressure recovery factor; Francis turbine; overall efficiency; velocity of flow; kinetic energy.

Reference to this paper should be made as follows: Kalidas, S., Rangasamy, R. and Seenivasan, V. (2023) 'Investigation on the 1-kW Francis turbine elbow type draft tube performance by numerical and optimisation approach', *Progress in Computational Fluid Dynamics*, Vol. 23, No. 1, pp.24–33.

Biographical notes: Sathish Kalidas is an Assistant Professor in the Department of Mechanical Engineering, Sri Eshwar College of Engineering, India. His research fields include optimisation and flow analysis in draft tube and turbine.

Ramamoorthi Rangasamy is an Associate Professor in the Department of Mechanical Engineering, Sri Krishna College of Engineering and Technology, India. His research fields include optimisation, composite materials and flow analysis in draft tube and turbine.

Venkatesh Seenivasan is a Post-Doctoral Fellow in the Department of Mechanical Engineering, National Institute of Technology, Tiruchirappalli, India. His research fields include optimisation, multiphase flow analysis in pollution control equipment.

1 Introduction

At present, petroleum and coal products are mostly utilised to produce energy. After a few years, these resources will be unable to meet the demands of the society owing to increasing energy consumption. In addition, environmental pollution and greenhouse effects are on the rise owing to the burning of coal and petroleum products (Muhirwa et al., 2019). Therefore, most countries are searching for alternative fuels to produce energy. Simultaneously, most researchers are focusing on improving the performance of renewable energy sources. Water is the best renewable energy resource for producing power because it emits less greenhouse gases. Moreover, it is a cost-effective resource for energy production. Therefore, most researchers are concentrating on improving the performance of hydrodynamic elements (Dekterev et al., 2015).

Kaplan, Francis, and Pelton are regularly used water turbines in hydropower plants. Among these, Francis turbines are the most preferred for medium-scale and microscale hydropower plants because they are suitable for operation in low and medium heads. They are also used in pico-hydropower plants (with power ranging from a few watts to 5-kW). The Francis turbine consists of a penstock, runner blades, stay ring, guide vanes, spiral casing, and draft tube. Usually, an elbow-type draft tube is utilised. It consists of a diffuser, hose, and elbow. The draft tube is connected at the exit of the runner, where the pressure is less than the atmospheric pressure. The exit velocity and kinetic energy of the water are reduced, and a gain in the useful pressure head is achieved when the water is passed through the draft tube. Hence, the working head and output power of the turbine are increased. The cross-sectional regions of the cone and diffuser are gradually enlarged in the draft tube to decrease the exit velocity. In addition, the area of the elbow is maintained constant to limit the loss caused by friction.

The performance of the draft tube is mostly impacted by its geometric parameters. Several researchers have attempted to improve the performance of the draft tube by altering the geometric parameters. The pressure recovery factor plays a significant role in increasing the proficiency of the draft tube. The various geometric factors of the draft tube were optimised using a surrogate model to increase the pressure recovery factor (Demirel et al., 2017). Moreover, the performance characteristics of the elbow draft tube were investigated by developing various types of arcs to describe the contours of the elbow geometry (Arispe et al., 2018). The effects of the vortex rope on the draft tube, exit velocity, and pressure fluctuations were investigated numerically and experimentally, and a method was proposed to evaluate the strength of the vortex rope (Cheng et al., 2020). Cross-flow turbines were utilised in micro-hydropower plants to produce energy. The performance of these turbines was theoretically analysed by introducing a guide tube into the draft tube (Abbas et al., 2020). Owing to flow instability in the draft tube, an undesirable pressure pulsation is created in the turbine, which significantly affects its performance. This objectionable pressure pulsation was evaluated using a comprehensive state index scheme to improve the hydraulic efficacy of the turbine (Wang et al., 2019). Chen et al. (2017) investigated the effect of the J-groove on draft tube performance. Ni et al. (2018) examined the flow field on a draft tube by applying a partial load with the aid of a vortex rope on the turbine. Muhirwa et al. (2020a) deliberated on the presence of pressure pulsation, vortex rope strength, and power swings in the draft tube, and suggested remedial actions to overcome these problems. The flow pattern inside the draft tube was experimentally investigated by Lai et al. (2019). In this investigation, the laser Doppler velocimetry (LDV) was utilised to analyse the flow pattern. Most researchers have applied the computational fluid dynamic (CFD) approach to explore the hydrodynamic activities of draft tubes (Muhirwa et al., 2020a, 2020b; Daniels et al., 2020; Kunniyoor et al., 2021). Few authors have applied various types of optimisation approaches to enhance the performance of the draft tubes (Chen et al., 2019; Su et al., 2020). The literature reports that the performance of the draft tube is affected by the reduced pressure recovery factor. The pressure recovery factor depends on the geometrical parameters of the draft tube.

In this study, a 1-kW Francis turbine draft tube is considered for optimisation. Three important geometric parameters of the draft tube are considered: hose length (H_1), diffuser length (H_2), and exit diameter of the diffuser (D_e). The Taguchi method is used to create the design matrix and regression equation. The pressure recovery factor is chosen as the response variable. The CFD approach is utilised to evaluate the pressure recovery factor for each combination of designs available in the design matrix. Subsequently, a genetic algorithm (GA) is executed to predict the optimum parameters. Finally, the optimum design of the draft tube is compared numerically and experimentally.

2 Reference model

A laboratory-scale experimental setup of the 1-kW Francis turbine was considered as the reference model, as depicted in Figure 1. The detailed dimensions of the Francis turbine draft tube are presented in Figure 2. In this setup, a 5-hp centrifugal pump was used to deliver water from the reservoir to the Francis turbine. The normal speed of the turbine was 2,200 rpm, and its maximum efficiency was 83.1%. The measured flow rate at the exit of the runner was 0.011 m^3/s. The measured inlet velocity at the bay port of the draft tube or departure of the runner was 1.6 m/s. At this velocity, the calculated pressure recovery factor was 0.75. The literature reports that the acceptable range of pressure recovery factor must be between 0.8 and 0.9 (Demirel et al., 2017). The predicted pressure recovery factor of the present reference model is 0.75, which is much less than the value prescribed in the literature. Further, the literature reports that the geometric parameters of the draft tube, namely, the hose length, diffuser length, and exit diameter of the diffuser, significantly impact the advancement of the

pressure recovery factor. Therefore, to improve the pressure recovery factor of the 1-kW turbine, these three parameters are considered for optimisation.

Figure 1 Experimental setup of the 1-kW Francis turbine (see online version for colours)

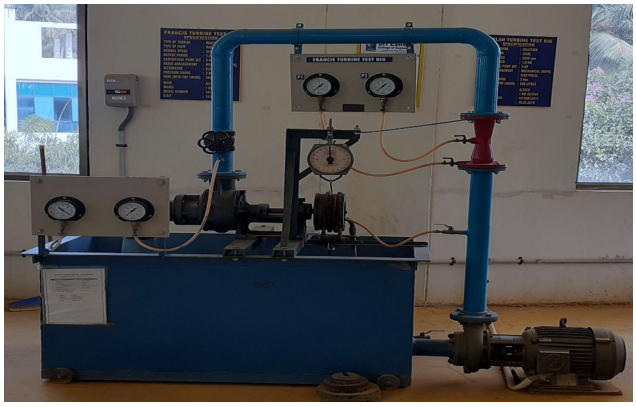

Figure 2 Dimensions of the 1-kW Francis turbine draft tube (see online version for colours)

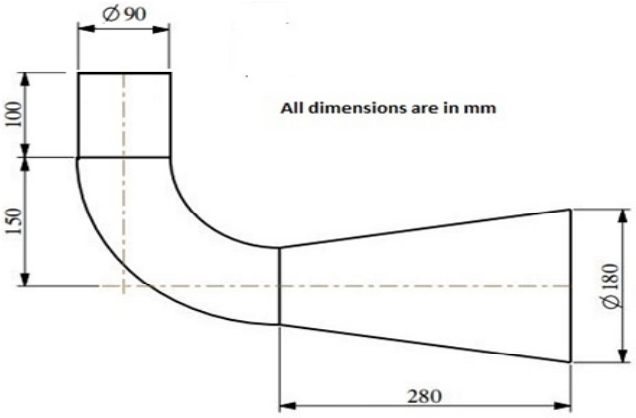

3 CFD analysis

3.1 Numerical settings and schemes

The shear stress transport (SST) *k-ω* model is most suitable for simulating flows with strong adverse pressure gradients and separation (Menter et al., 2003). This turbulence model is applied to address complex-flow problems in several industrial applications, such as transonic shock waves, airfoils, and adverse pressure gradient flows. Moreover, the addition of a blending function and cross-diffusion term in the ω equation allows this model to perform properly in both the far-field and near-wall regions (Menter et al., 2003; Menter and Egorov, 2010). The SST *k-ω* turbulence model is an eddy viscosity two-equation model, which applies the *k-ε* scheme in the free-flow region as well as in the boundary layer regions by way of blending functions. The functional magnitude deviates from 0 (far from the wall) to 1 (near the wall) (Arispe et al., 2018). Thus, this model produces more precise results for adjacent wall streams with adverse pressure gradients. Therefore, previously, several researchers have prescribed the SST *k-ω* scheme for the simulation of the Francis turbine draft tube (Galvan et al., 2011; Abbas and Kumarm, 2017; Arispe et al., 2018; Cheng et al., 2020; Islam et al., 2020). Thus, the SST *k-ω* turbulence model is utilised in the present simulation to solve the 3D Reynolds-averaged Navier-stokes (RANS) equations for a stable-state incompressible flow. The Ansys Fluent 15.0 package is utilised for the simulation.

The Navier-Stokes equations for an incompressible fluid flow are as follows.

The continuity equation is expressed as follows:

$$\frac{\partial U_i}{\partial x_i} = 0 \tag{1}$$

The momentum equation can be expressed as follows (Fluent, Inc., 2004):

$$\frac{\partial U_i}{\partial t} + U_j \frac{\partial U_i}{\partial x_j} = -\frac{\partial \overline{p}/\rho}{\partial x_i} + \nu \frac{\partial^2 U_i}{\partial x_j \partial x_j} - \frac{\partial}{\partial x_j}\left(\overline{u_i' u_j'}\right) \tag{2}$$

where $u_i' u_j'$, , is expressed as

$$\overline{u_i' u_j'} = \nu_t \left(\frac{\partial U_i}{\partial x_j} + \frac{\partial U_j}{\partial x_i}\right) - \frac{1}{3}\overline{u_i' u_i'}\delta_{ij} \tag{3}$$

The equation for the SST *k-ω* turbulence model can be expressed as follows (Fluent, Inc., 2004):

$$\frac{\partial}{\partial t}(\rho k) + \frac{\partial}{\partial x_i}(\rho k u_i) = \frac{\partial}{\partial x_j}\left(\Gamma_k \frac{\partial k}{\partial x_j}\right) + \tilde{G}_k - Y_k + S_k \tag{4}$$

$$\frac{\partial}{\partial t}(\rho \omega) + \frac{\partial}{\partial x_i}(\rho \omega u_i) = \frac{\partial}{\partial x_j}\left(\Gamma \omega \frac{\partial \omega}{\partial x_j}\right) + G_\omega - Y_\omega + D_\omega S_\omega \tag{5}$$

where Γ_k, Γ_ω are the effective diffusivities, expressed as

$$\Gamma_k = \mu + \frac{\mu_t}{\sigma_k} \tag{6}$$

$$\Gamma_\omega = \mu + \frac{\mu_t}{\sigma_\omega} \tag{7}$$

where F_1 and F_2 are blending functions, expressed as

$$F_1 = \tanh\left(\Phi_1^4\right) \tag{8}$$

$$F_2 = \tanh\left(\Phi_2^2\right) \tag{9}$$

The production of the turbulence kinetic energy can be expressed as follows:

$$\tilde{G}_k = \min\left(G_k, 10\rho\beta * k\omega\right) \tag{10}$$

The production of ω can be expressed as follows:

$$G_\omega = \frac{\alpha}{\nu_t} G_k \tag{11}$$

$$Y_k = \rho\beta * k\omega \tag{12}$$

where Y_k is the dissipation of the turbulence kinetic energy.

$$Y_\omega = \rho\beta\omega^2 \tag{13}$$

where Y_ω is the dissipation of ω, and β is a constant.

$$\sigma_{k,1} = 1.176,\ \sigma_{\omega,1} = 2.0,\ \sigma_{k,2} = 1.0,\ \sigma_{\omega,2} = 1.168$$

$$a_1 = 0.31,\ \beta_{i,1} = 0.075,\ \beta_{i,2} = 0.0828$$

The pressure–velocity coupling was treated using the pressure implicit with splitting of operators (PISO) scheme. In addition, a second-order upwind scheme was adopted for the specific dissipation rate, turbulence kinetic energy, and momentum. The first-order implicit scheme was adopted for the transient formulation. A time-dependent solution was used as a method of integration to achieve a steady-state solution. The calculation was initiated with a steady-state solution. The solution was not converged as a result of 1,000 iterations performed in steady-state. Therefore, the transient simulation was initiated after 1,000 steady-state iterations, taking the flow field resulting after 1,000 steady-state iterations as the initial condition. For monitoring the periodicity, separate windows were opened for residuals, pressure contour, velocity contour and kinetic energy contour. The residual value of the variables was established as 10^{-4} for accurate convergence, which is sufficient to obtain the field of the flow. The periodicity was determined after reaching the stable condition in this residual plot and flow field results. The time-averaging was started after this condition. In this simulation, the time-averaged results for the transient state was selected from 4.5 s to 6 s time interval (averaged results for 1.5 s has been selected). In this simulation, the time step size was given as 0.01 s. The maximum number of iterations per time step is 20. The total flow time in this simulation is 6 s. The number of time step has been selected based on monitoring the residual and flow field results in separate windows. It is observed that the stable condition was reached at flow time of 6 s. In this simulation, the periodicity or repetition of value in results was started from 450 time steps and the calculation was ended in 600 time steps. The calculation was ended at 6,650 iterations in transient condition (6,650 iterations in transient and 1,000 iterations in steady-state).

The time-averaged pressure profiles were plotted for optimisation, and the pressure recovery factor was calculated based on these results. The turbine was not considered in the simulation, and only the draft tube was modelled and simulated. The literature suggests that the first-order implicit scheme is sufficient to achieve quick convergence in this type of simulation. Hence, in this simulation, a first-order implicit scheme is utilised to achieve easy convergence in the results.

3.2 Boundary condition

The mass flow inlet boundary condition (normal to the boundary) was selected for the draft tube inlet. From the experimental analysis, the measured flow rate at the exit of the runner was calculated as 0.011 m^3/s. Hence, this value was considered for the inlet boundary condition. The turbulence intensity and hydraulic diameter values for the entry port of the draft tube were specified as 5% and 0.09 m, respectively. The pressure outlet option was specified for the exit port of the draft tube. The remaining surfaces of the draft tube were set to the no-slip boundary condition. The density of water specified in the present simulation was 1,000 kg/m^3.

3.3 Mesh generation and validation

The solid model of the draft tube was developed using the PTC-CREO modelling package and exported as an Initial graphics exchange (IGS) file format. A hexahedral mesh was developed using the finite-volume method for the draft tube in the reference model, as illustrated in Figure 3. Fine hexahedral grids were generated to avoid computational uncertainty. A fine relevance centre and high smoothing choice were selected for generating the fine grids. The number of grid elements created in this simulation was 152,426. The number of nodes developed was 173,256. The transition ratio and curvature angle were set as 0.272 and 18°, respectively. The mesh quality was validated through a grid independence study (GIS). In the GIS, three different sets of grids were produced: 67,246, 101,524, and 152,426. The pressure recovery factor was predicted for these three sets of grids. The details of the GIS are presented in Table 1. Richardson's theory states that the refinement ratio must be higher than 1.3 (Slack et al., 2000). In this simulation, the refinement ratio between the first and second sets of grids was 1.5. Further, the refinement ratio between the second and third sets of grids was 1.52. The percentage variance between the first and second meshes was 0.79% in relation to the pressure recovery factor results. In addition, the percentage variance between the second and third meshes was 0.52% in relation to the pressure recovery factor results, which is less than 1%. A larger number of grids, such as 152,426, was considered to avoid computational insecurity. These outcomes indicate that the grids used for conducting the simulation were of excellent quality.

The near-wall turbulence was treated using a near-wall modelling approach. To resolve the mean velocity and turbulence quantities in this region, 15 layers were created within the viscosity-affected near-wall region using the inflation option. The growth rate was considered to be 1.2. For the SST *k-ω* model, $y^+ \leq 2$ is recommended for near-wall resolution in industrial complex-flow applications (Menter et al., 2003). The y^+ value obtained next to the wall cells was 0.86. Based on the literature, this value satisfies the requirements of the applied near-wall treatment. A grid diagram is presented in Figure 3.

Table 1 Details of the GIS

Mesh	*No. of elements*	*Pressure recovery factor (c_p)*
M1	67,246	0.745
M2	101,524	0.751
M3	152,426	0.755

Figure 3 Mesh for the draft tube in the reference model

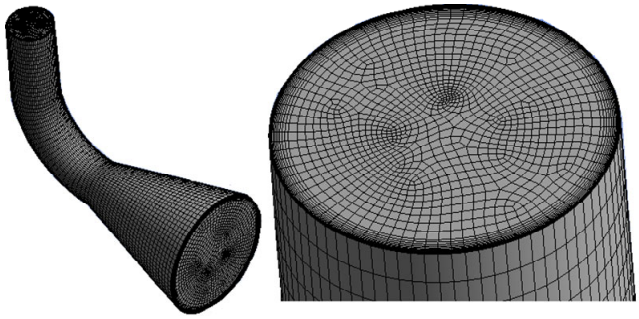

3.4 Validation of CFD results

The fabrication of a number of draft tubes for experimental analysis increases the cost of investigation. Therefore, the objective function (pressure recovery factor) for the various design combinations of the draft tube to be predicted by the CFD analysis in this study. Hence, the CFD results were validated using the experimental results before conducting the design of experiment (DoE) analysis. The pressure recovery factor for the 1-kW Francis turbine draft tube was predicted for various flow rates through experimental and CFD analyses. The results are presented in Figure 4. The operating conditions considered in the CFD and experimental analyses were identical. The validation results indicate that an acceptable range of accuracy was obtained in the CFD simulation. Hence, the present simulation conditions and schemes were suitable for predicting the objective functions required for conducting the DoE and optimisation.

Figure 4 Validation results of draft tube (see online version for colours)

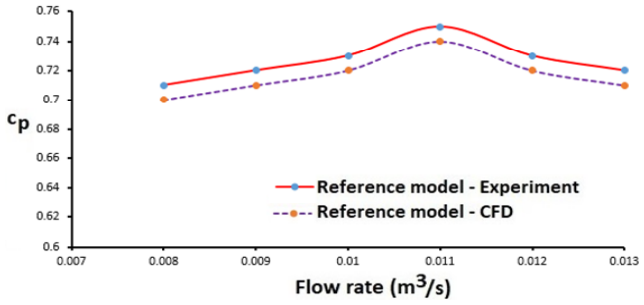

3.5 Design of experiment

Taguchi is a measurable strategy used to improve the quality of engineering components utilised in various fields. Recently, this technique has been effectively utilised in various fields of design. This strategy is increasingly being utilised in the production and modern designing fields for improving the exhibition of existing frameworks through streamlined plan boundaries (Roy, 1990). Further, it is appropriate for developing a linear mathematical equation for optimisation. In the present study, the three vital geometric parameters of the draft tube, namely, the hose length, diffuser length, and exit diameter of the diffuser, were considered for developing the regression equation. The pressure recovery factor (c_p) was considered as the response parameter. Three levels (minimum, medium, and maximum) were considered for each geometric parameter of the draft tube for developing the L_9 orthogonal array. The parameters and their minimum, medium, and maximum levels are listed in Table 2.

Table 2 Geometric parameters and their levels

Parameters	*Level 1*	*Level 2*	*Level 3*
Hose length (H_1)	100	130	160
Diffuser length (H_2)	280	310	340
Exit diameter of the diffuser (D_e)	180	210	240

3.5.1 L_9 orthogonal array and Taguchi analysis

The design matrix was developed using the L_9 orthogonal array based on the three levels and the three parameters. In the matrix, nine combinations of the geometric parameters of the draft tube were developed, as listed in Table 3. The Minitab-17 statistical tool was utilised for developing the matrix. The fabrication of nine draft tubes for the experimentation would increase the analysis cost and time. Therefore, instead of conducting physical experiments, the CFD approach was utilised to predict the response parameters. The pressure recovery factor was computed for these nine design combinations of the draft tube using CFD analysis. To compute the pressure recovery factor, it is essential to compute the static pressure variance between the entrance and exit ports of the draft tube. Subsequently, the pressure recovery factor was calculated using equation (14) (Demirel et al., 2017):

$$C_P = \frac{P_{out,s} - P_{in,s}}{0.5\,\rho V_{in}^2} \tag{14}$$

The predicted static pressure contours of the nine draft tubes are presented in Figure 5. The simulation procedure and settings for the CFD analysis are discussed in Subsection 3.1. The literature reports that increasing the pressure recovery factor increases the hydraulic efficiency of the turbine. Therefore, the-larger-the-better choice is specified for maximising the pressure recovery factor. Moreover, the signal-to-noise ratio (SNR) was computed for each pressure recovery factor with respect to each design combination. The mean effect plot was generated based on the SNR values and geometric parameters. The plot is presented in Figure 6. It indicates that increasing the size of the geometric factors of the draft tube, namely, H_1, H_2, and D_e, significantly affects the pressure recovery factor. The SNR is computed using the following equation (Roy, 1990):

$$\eta = -10\log_{10}\frac{1}{n}\sum\frac{1}{Y_i^2} \tag{15}$$

Subsequently, the regression equation was predicted for the optimisation of the geometric factors of the draft tube. The linear regression equation developed through the Taguchi analysis is expressed in equation (16):

$$c_p = 0.516 + 0.001111H_1 - 0.000167H_2 + 0.000944D_e \quad (16)$$

Table 3 L_9 orthogonal array and SNR

S. no.	H_1	H_2	D_e	c_p	*S/N ratio*
1	100	280	180	0.75	–2.49877
2	100	310	210	0.77	–2.27019
3	100	340	240	0.78	–2.15811
4	130	280	210	0.82	–1.72372
5	130	310	240	0.84	–1.51441
6	130	340	180	0.8	–1.93820
7	160	280	210	0.85	–1.11035
8	160	310	180	0.78	–2.15811
9	160	340	240	0.84	–1.51441

Figure 5 Static pressure contours for the L_9 array (see online version for colours)

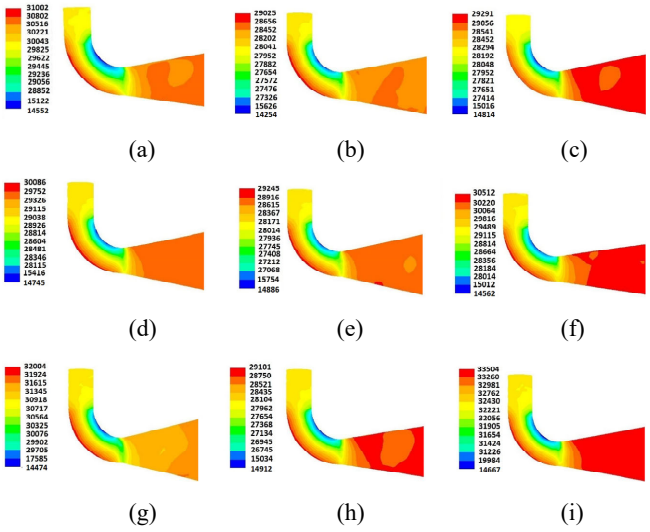

Figure 6 Plot presenting the parameters vs. SNR (see online version for colours)

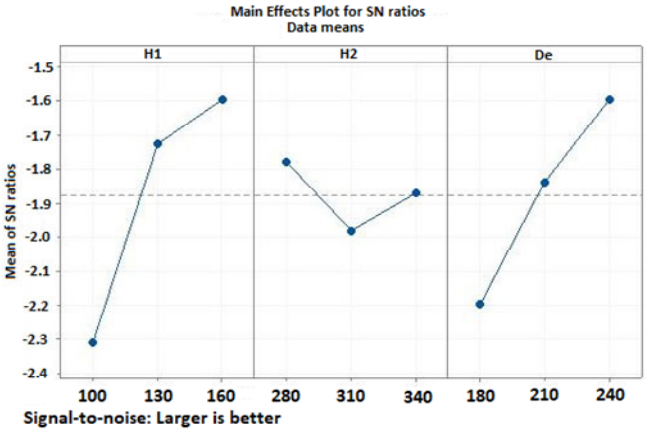

3.5.2 Analysis of variance

The quality of the regression equation was validated using the analysis of variance (ANOVA). In the ANOVA, the P-test and F-test were conducted against each geometric factor. The results indicated that H_1 and D_e significantly affected the pressure recovery factor ($P < 0.05$). In contrast, H_2 had an insignificant effect on the pressure recovery factor ($P < 0.05$). The P-value for regression falls below 0.05, which indicates that the developed mathematical model is suitable for optimisation. The predicted R-Sqr and R-Sqr (adj.) values were 91% and 90.2%, respectively. These results confirm that the developed regression model is excellent for optimisation. The results of the ANOVA are presented in Table 4.

Table 4 ANOVA results

Source	*DF*	*Adj. SS*	*Adj. MS*	*F-value*	*P-value*
Regression	3	0.011633	0.003878	8.95	0.019
H_1	1	0.006667	0.006667	15.38	0.011
H_2	1	0.000150	0.000150	0.35	0.582
D_e	1	0.004817	0.004817	11.12	0.021
Error	5	0.002167	0.000433		
Total	8	0.013800			

4 Genetic algorithm

The GA was invented by John Holland in 1960. It is a non-traditional optimisation method. Currently, it is used in the design of machine elements, production, planning, and manufacturing sectors to obtain optimised results for improving the quality (Michalevicz, 1992; Reeves, 1997). In this study, the GA was utilised to optimise the geometric parameters of the draft tube to improve the pressure recovery factor. The fitness function equation was derived through the Taguchi analysis, and is expressed in equation (16). MATLAB version 18 software was used to perform the GA optimisation. Initially, an m-file was created to commence the GA. An objective function was written into this file based on the derived regression equation [equation (17)]:

1 Function $Z = f(Y)$.

2
$$Z = 0.516 + 0.001111 * Y(1) - 0.000167 * Y(2) + 0.000944 * Y(3). \quad (17)$$

The GA settings were provided in the optimisation tool after creating this objective function in the m-file. The double vector population was selected, and the size of the population was set as 30. Thereafter, a uniform creation function was selected. The lower bound values were set to [100, 280, 180]. The upper bound values were set to [160, 340, 240]. Subsequently, rank-type fitness scaling was selected. A single-point crossover function was chosen for the simulation, and its fraction was set as 2. In addition, a uniform mutation was chosen, and its rate was provided as a default. Forward migration was selected to perform the optimisation. The number of generations was 100. The stall limit was set to 50. After setting all the simulation parameters, the optimisation was continued until the solution converged. After attaining convergence, the current

best individual values were predicted, which were 0.881 and 0.886. The optimum parameters of the draft tube are listed in Table 5.

Table 5 Optimised results

Variables	*Hose length (H_1)*	*Diffuser length (H_2)*	*Exit diameter of the diffuser (D_e)*
Dimension (mm)	160	280	240

5 Results and discussion

5.1 Pressure field

The static pressure flow fields of the reference and optimum model draft tubes are depicted in Figure 7. Equation (14) clearly indicates that the pressure recovery factor is directly proportional to the static pressure variance between the entrance and exit ports of the draft tube (Demirel et al., 2017). Therefore, increasing the static pressure difference between the entrance and exit ports of the draft tube increases the pressure recovery factor. Moreover, the pressure recovery factor was indirectly proportional to the velocity. Therefore, decreasing the exit velocity at the draft tube increases the pressure recovery factor. A 1-kW Francis turbine draft tube was considered for the investigation. This turbine produced a maximum pressure recovery factor at a flow rate of 0.011 m^3/s. The measured velocity of the flow at the inlet of the turbine or exit of the runner was 1.6 m/s (from the experiment).

The contour plots indicate that the static pressure increased towards the exit of the draft tube. In both models, the exit pressure was higher when compared with the inlet of the draft tube. Moreover, the pressure reached the minimum value in the inner circle of the elbow. Furthermore, the pressure increased at the outer circle of the elbow. The pressure was slightly higher at the inner and exterior radii of the elbow in the optimum design when compared with the reference model. The exit pressure at the optimum design was higher when compared with the reference model. This indicates that the static pressure variance between the entrance and exit ports of the optimum design was higher when compared with the reference model considered in this study. The pressure recovery factor was calculated using equation (14) based on the difference in the static pressure. The calculated and predicted pressure recovery factors for the reference model and optimised design, respectively, were 0.75 and 0.88. The pressure recovery factor of the optimum design was 14.7% higher when compared with the reference design. The pressure recovery factor was computed for different flow rates, as depicted in Figure 8. The volumetric flow was adjusted from 0.008 to 0.013 m^3/s to calculate the pressure recovery factor. The least pressure recovery factor was available at a volumetric flow of 0.008 m^3/s. Furthermore, the recovery factor reached a maximum at 0.011 m^3/s. A further increase in the flow rate decreased the recovery factor. In the optimum design, H_1 was increased from 100 to 160 mm. The pressure increased at the inlet hose owing to this increase in length. Further, the value of D_e was increased from 180 to 240 mm. The results indicate that the pressure increased at the exit port of the diffuser in the optimum design when compared with the reference design.

Figure 7 Contours for static pressure (Pa), velocity (m/s), and turbulence kinetic energy (m^2/s^2), (a) reference model (b) optimum model (see online version for colours)

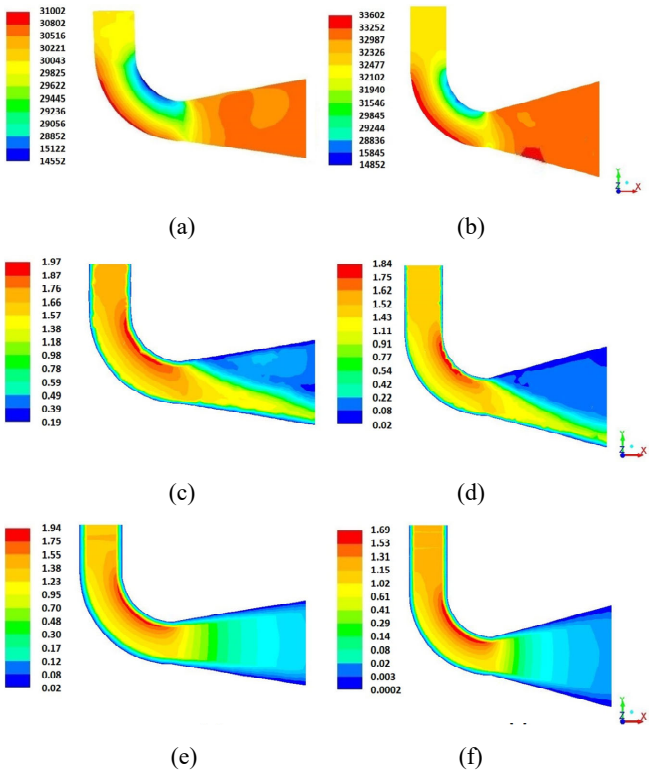

Figure 8 Comparison of pressure recovery factor (see online version for colours)

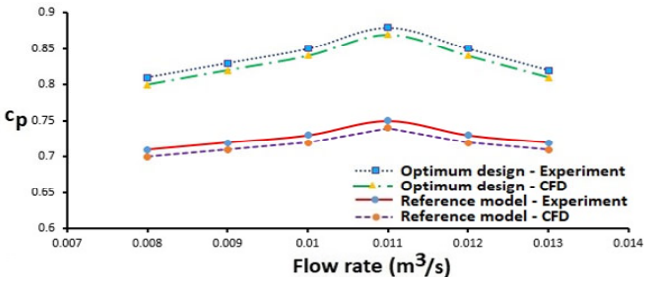

5.2 Velocity field

The velocity flow field of the draft tube is depicted in Figure 7. This contour plot indicates that the exit velocity of the flow decreased (almost to zero) at the exit port of the draft tube when compared with the inlet velocity. The pressure recovery factor was indirectly proportional to the velocity of flow (Demirel et al., 2017). This confirms that the static pressure increased in the exit port of the draft tube. The velocity of flow increased at the internal radius of the elbow, which caused the pressure to decrease at this location. In contrast, the velocity of flow decreased at the

external radius of the elbow. This caused the pressure to increase at the outer radius of the elbow. The separation of flow occurred because of this velocity difference at the convex and concave surfaces of the elbow. Therefore, the frictional loss diminished in this region. The difference in velocity at the elbow of the optimum design was less when compared with the reference model. Further, the area of the diffuser increased towards the exit port. Therefore, the velocity decreased at the exit area of the diffuser. Thus, in the optimum design, the exit size of the diffuser increased. Therefore, the velocity is lower at the exit port of the optimum design when compared with the reference model. These results confirm that the pressure recovery factor increased in the optimum design.

5.3 Turbulence kinetic energy

The turbulence kinetic energy flow fields are depicted in Figure 7. The kinetic energy of the flow decreased in the exit port of the draft tube. The kinetic energy increased at the internal radius of the elbow in both the draft tubes. This confirms that a maximum velocity existed in this region. Moreover, the kinetic energy decreased at the outer radius of the elbow; in this region, the velocity was slightly decreased. Further, the velocity significantly decreased towards the exit port of the diffuser. Therefore, the kinetic head decreased significantly at the exit port of the diffuser. The available net turbulence kinetic energies in the reference and optimum model draft tubes were 1.53 and 1.12 m^2/s^2, respectively. The kinetic energy in the optimised draft tube was reduced by 26.7% when compared with the reference draft tube. This indicates that the optimised draft tube improved the performance of the turbine

5.4 Comparison of efficiency

The new draft tube was fabricated based on the optimised results for conducting the confirmation test. The fabricated draft tube is illustrated in Figure 9. Subsequently, this draft tube was connected to the 1-kW Francis turbine experimental setup to predict the overall efficiency. The flow rate was adjusted from 0.008 to 0.013 m^3/s and a constant speed of 2,200 rpm was maintained to predict the overall efficiency. The overall efficiency increased up to 0.011 m^3/s. When the optimised draft tube was connected to the Francis turbine, the predicted maximum overall efficiency was 94.4% at 0.011 m^3/s. To analyse the repeatability, three trials were conducted in this experimental analysis under identical operating conditions, such as a flow rate of 0.011 m^3/s. They yielded more or less identical results. The maximum error percentage between these trials was less than 1%. From these three trials, that with the maximum efficiency (94.4%) was chosen to generate the results. Further, the overall efficiency of the existing model was 83.1%. Evidently, by using the optimum draft tube, the overall efficiency had increased by 11.9%. The overall efficiency versus the flow rate plot is presented in Figure 10. The overall efficiency decreased owing to a further increase in the flow rate (above 0.011 m^3/s). The total head predicted using the reference draft tube was 8.8 m. In contrast, the total head predicted using the optimum draft tube was 8.3 m. The decrease in the total head owing to the optimum draft tube was 5.6%. The output powers developed in the turbine shaft owing to the optimum and existing draft tubes were 0.85-kW and 0.79-kW, respectively. The results of the comparison are summarised in Table 6.

In the optimum design, H_1 was increased from 100 to 160 mm. The pressure at the inlet hose increased owing to this increase in length. Further, D_e was increased from 180 to 240 mm. The results indicate that the pressure at the exit port of the diffuser in the optimum design increased when compared with the reference design. The overall efficiency increased by 11.9% owing to the geometrical alteration of the elbow draft tube. The pressure recovery factors for the optimum design and reference model were 0.88 and 0.75, respectively. Thus, there was an increase of 14.7% in the pressure recovery factor owing to the optimum draft tube.

Figure 9 Fabrication of optimised draft tube (see online version for colours)

Figure 10 Results of the comparison of the overall efficiency (see online version for colours)

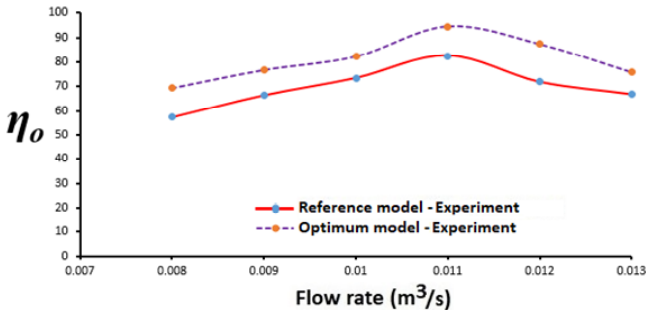

Table 6 Comparison of the overall efficiency

Model	*Flow rate (Q) m^3/s*	*Total head (H) m*	*Speed (N) Rpm*	*Resultant load (T) kg*	*Input power (kW)*	*Output power (kW)*	*Efficiency (η_o)%*
Reference	0.011	8.8	2,200	3.3	0.95	0.79	83.1
Optimum	0.011	8.3	2,200	3.5	0.9	0.85	94.4

6 Conclusions

In this investigation, the geometric parameters of the draft tube, namely, the hose length, diffuser length, and exit diameter of the diffuser, were altered using the GA. The results of the GA indicated that increasing the hose length from 100 to 160 mm produced a better effect on the pressure recovery factor. Moreover, increasing the exit diameter of the draft tube significantly affected the pressure recovery factor. In contrast, the diffuser length did not affect the pressure recovery factor. Among these three process parameters, an increase in the hose length significantly affected the pressure recovery factor. The optimum results indicate that the hose length increased from 100 to 160 mm. Moreover, an increase in the exit diameter of the diffuser significantly affected the pressure recovery factor. However, an increase in the hose length produced a 47.6% higher effect on the pressure recovery factor when compared with the exit diameter of the diffuser. Hence, the hose length of the draft tube was identified as the parameter that strongly impacted the output response. Altering the geometrical factors of the draft tube increased the overall efficiency of the Francis turbine. The overall efficiency increased by 11.9% owing to the geometrical alteration of the elbow draft tube. The optimum draft tube produced an overall efficacy of 94.4%. The pressure recovery factor for the optimum design was 0.88. In addition, the pressure recovery factor for the reference model was 0.75. Thus, the pressure recovery factor was found to be increased by 14.7% using the optimum draft tube. The pressure recovery factor, velocity field, and kinetic energy field were predicted using the CFD analysis. Moreover, the pressure recovery factor predicted using the CFD analysis was compared with the experimental results, and the comparison produced satisfactory results.

References

Abbas, A. and Kumarm, A. (2017) 'Development of draft tube in hydro-turbine: a review', *International Journal of Ambient Energy*, Vol. 38, No. 3, pp.323–330.

Abbas, A., Alam, M. and Kumar, R. (2020) 'Analytical analysis of combined effect of interior guide tube and draft tube on cross flow turbine performance', *Materials Today Proceedings*, pp.1–6 [online] http://doi.org/10.1016/j.matpr.2020.08.796.

Arispe, T.M., Oliveira, W.D. and Ramirez, R.G. (2018) 'Francis turbine draft tube parameterization and analysis of performance characteristics using CFD techniques', *Renew Energy*, Vol. 127, pp.114–124.

Chen, Z., Baek, S.H. and Cho, H. (2019) 'Optimal design of J-groove shape on the suppression of unsteady flow in the Francis turbine draft tube', *Journal of Mechanical Science and Technology*, Vol. 33, No. 5, pp.2211–2218.

Chen, Z., Singh, P.M. and Choi, Y.D. (2017) 'Suppression of unsteady swirl flow in the draft tube of a Francis hydro turbine model using J-groove', *Journal of Mechanical Science and Technology*, Vol. 31, No. 12, pp.5813–5820.

Cheng, H., Zhou, L., Liang, Q., Guan, Z., Liu, D., Wang, Z. and Kang, W. (2020) 'A method of evaluating the vortex rope strength in draft tube of Francis turbine', *Renew Energy*, Vol. 152, pp.770–780.

Daniels, S.J., Rahat, A.A.M., Tabor, G.R., Fieldsend, J.E. and Everson, R.M. (2020) 'Shape optimization of the sharp-heeled Kaplan draft tube: performance evaluation using computational fluid dynamics', *Renew Energy*, Vol. 160, pp.112–126.

Dekterev, A.A., Zakharov, A.V., Minakov, A.V., Platonov, D.V. and Pylev, I.M. (2015) 'Mathematical modeling of low-frequency pressure fluctuations in hydroturbine ducts', *Fluid Dynamics*, Vol. 50, pp.601–612.

Demirel, G., Acar, E., Celebioglu, K. and Aradag, S. (2017) 'CFD-driven surrogate-based multi-objective shape optimization of an elbow type draft tube', *International Journal of Hydrogen Energy*, Vol. 42, No. 28, pp.17601–17610.

Fluent, Inc. (2004) *Fluent 6.1.22 Users' Guide*.

Galvan, S., Reggio, M. and Guibault, F. (2011) 'Assessment study of *k-e* turbulence models and near-wall modeling for steady state swirling flow analysis in draft tube using fluent', *Engineering Applications of Computational Fluid Mechanics*, Vol. 5, No. 4, pp.459–478.

Islam, S.M., Khan, M.T. and Ahmed, Z.U. (2020) 'Effect of design parameters on flow characteristics of an aerodynamic swirl nozzle', *Progress in Computational Fluid Dynamics, An International Journal*, Vol. 20, No. 5, pp.249–262.

Kunniyoor, V., Singh, P. and Nadella, K. (2021) 'Aerodynamic design and computational fluid dynamic analysis of radial outflow turbines for steam Rankine cycle and supercritical carbon dioxide Brayton cycle', *Progress in Computational Fluid Dynamics, An International Journal*, Vol. 21, No. 2, pp.65–90.

Lai, X.D., Liang, Q.W., Ye, D.X., Chen, X.M. and Xia, M.M. (2019) 'Experimental investigation of flows inside draft tube of a high-head pump-turbine', *Renew Energy*, Vol. 133, No. 1, pp.731–742.

Menter, F. and Egorov, Y. (2010) 'The scale-adaptive simulation method for unsteady turbulent flow predictions. Part 1: theory and model description', *Flow, Turbulence and Combustion*, Vol. 85, No. 1, pp.113–138.

Menter, F., Kuntz, M. and Langtry, R. (2003) 'Ten years of industrial experience with the SST turbulence model', *Heat Mass Transfer*, Vol. 4, pp.1–9.

Michalevicz, Z. (1992) *Genetic Algorithms + Data Structures = Evolution Programs*, Springer. New York.

Muhirwa, A., Cai, W.H., Li, F.C., Su, W.T., Binama, M., Li, B. and Li, X.B. (2019) 'Investigation into the outlying swirl instability in the hydro-turbine draft tube under part-load operation', *Proceedings of the Institution of Mechanical Engineers, Part A: Journal of Power and Energy*, Vol. 235, No. 1, pp.139–153.

Muhirwa, A., Cai, W.H., Su, W.T., Liu, Q., Binama, M., Li, B. and Wu, J. (2020a) 'A review on remedial attempts to counteract the power generation compromise from draft tubes of hydropower plants', *Renew Energy*, Vol. 150, pp.743–764.

Muhirwa, A., Li, B., Su, W.T., Liu, Q.Z., Binama. M., Wu, J. and Cai, W.H. (2020b) 'Investigation on mutual traveling influences between the draft tube and upstream components of a Francis turbine unit', *Renew Energy*, Vol. 162, pp.973–992.

Ni, Y., Zhu, R. and Zhang, X. (2018) 'Numerical investigation on radial impeller induced vortex rope in draft tube under partial load conditions', *Journal of Mechanical Science and Technology*, Vol. 32, No. 1, pp.157–165.

Reeves, C.R. (1997) 'Genetic algorithms for the operation researcher', *INFORMS Journal on Computing*, Vol. 9, No. 3, pp.231–250.

Roy, R.K. (1990) *Design of Experiments using the Taguchi Approach*, John Wiley & Sons, New York.

Slack, M.D., Prasad, R.O., Bakker, A. and Boysan, F. (2000) 'Advances in cyclone modeling using unstructured grids', *Trans IChemE*, Vol. 78, No. 8, pp.1098–1104.

Su, W.T., Binama, M., Li, Y. and Zhao, Y. (2020) 'Study on the method of reducing the pressure fluctuation of hydraulic turbine by optimizing the draft tube pressure distribution', *Renew Energy*, Vol. 162, pp.550–560.

Wang, W., Chen, Q., Yan, D. and Geng, D. (2019) 'A novel comprehensive evaluation method of the draft tube pressure pulsation of Francis turbine based on EEMD and information entropy', *Mechanical Systems and Signal Processing*, Vol. 116, No. 1, pp.772–786.

Nomenclature

Latin letters	
C_P	Pressure recovery factor
D_e	Exit diameter of the diffuser (mm)
D_ω	Cross-diffusion term
F_1, F_2	Blending functions
G_ω	Generation of ω
$\tilde{G}_k$	Generation of turbulence kinetic energy
H_1	Hose length (mm)
H_2	Diffuser length (mm)
k	Turbulence kinetic energy (m^2/s^2)
n	Number of observations
$P_{out,s}$	Static pressure at outlet (Pa)
$P_{in,s}$	Static pressure at inlet (Pa)
$\bar{p}$	Static pressure (Pa)
S_k, S_ω	User-defined source terms
T	Resultant load (kg)
u_i, u_j, u_k	Velocity component in corresponding direction (m/s)
$u_i^{'}$, $u_j^{'}$	Fluctuating velocity (m/s)
U_i, U_j	Mean velocity along the i^{th} and j^{th} direction (m/s)
V_{in}	Inlet velocity of fluid (m/s)
x_i, x_j	Position along i^{th} and j^{th} direction (m)
Y_i	n observations of response variable
Y_k	Dissipation of turbulence kinetic energy

Nomenclature (continued)

Latin letters	
Y_ω	Dissipation of ω
Y	Input variables
y^+	Non-dimensional wall-normal distance
Z	Response variable
Greek symbols	
ρ	Density of fluid (kg/m^3)
$a_1\alpha$, β	Empirical coefficients for k-ω SST turbulence mode
Γ_k	Effective diffusivity of k
Γ_ω	Effective diffusivity of ω
μ	Fluid viscosity (kg/ms)
ν	Kinematic viscosity (m^2/s)
δ_{ij}	Kronecker delta function
η	Signal to-noise ratio
ω	Specific dissipation rate (1/s)
Φ	Scalar variable
ε	Turbulence dissipation rate (m^2s^{-3})
ν_t	Turbulence kinematic viscosity (m^2/s)
μ_t	Turbulence viscosity (Pa.s)
σ_k, σ_ω	Turbulence Prandtl numbers for k and ω
Sub and superscripts	
e	Exit
In	Inlet
Out	Outlet
i, j, k	Subscripts denoting Cartesian coordinate directions or index 1, 2, 3
t	Turbulence
p	Pressure
Abbreviations	
ANOVA	Analysis of variance
CFD	Computational fluid dynamics
DoE	Design of experiment
GA	Genetic algorithm
GIS	Grid independence study
IGS	Initial graphics exchange
LDV	Laser Doppler velocimetry
PISO	Pressure implicit with splitting of operators
RANS	Reynolds-averaged Navier-stokes
SNR	Signal-to-noise ratio
SST	Shear stress transport